JPEDAV (2006) 27:469-476
DOI: 10.1361/154770306X132001
1547-7037/$19.00 ©ASM International

The 450 °C Isothermal Section of the Zn-Al-Mo Phase Diagram

Zhihong Wang, Jianhua Wang, Nai-Yong Tang, Yi Hui Liu, and Xuping Su

(Submitted March 13, 2006; in revised form June 12, 2006)

The 450 °C isothermal section of the Zn-Al-Mo phase diagram has been determined experimentally using scanning electron microscopy (SEM) coupled with energy dispersive x-ray spectroscopy and x-ray diffractometry. The focus of the work is the Zn-rich corner due to its relevance to galvanizing. The present study indicates that with the increasing Al content of alloys, the liquid phase is successively in equilibrium with the ternary extensions of intermetallic compounds of $MoZn_{22}$, $MoZn_7$, $AlMo_3$, and Al_8Mo_3.

Keywords equilibrium, galvanizing, microstructure, ternary phase diagram, Zn-Al-Mo

1. Introduction

Zinc and Zn alloy coatings have long been used to protect steels from corrosion. The hot dip process is the most economic way to apply Zn coatings, and continuous galvanizing lines are able to produce coated strip with well-controlled coating thickness and uniformity.

A few types of coatings, such as galvanneal (GA), galvanized (GI), Galfan (GF), and Galvalume (GL), are commercially produced for various applications. In continuous galvanizing, Al is the most important alloying element of the bath and different Al levels are required to produce different types of coatings.[1] The molten Zn-Al alloys are extremely corrosive to metallic materials.[2,3] As a result, pot hardware, such as sink rolls, stabilizer rolls, and their bearings, are subjected to severe wear and corrosion in service. Frequent line stoppage for hardware replacement is the bottleneck in line operating efficiency improvement. Corrosion of rolls in GA and GI production can be largely overcome by applying a coating to the roll surfaces. However, in galvanizing involving a high bath temperature and a high Al content, such as GL, the commonly used tungsten carbide (WC) based coating does not perform well. Instead, Mo-base alloys, such as Mo-W and Mo-W-Cr, are used as roll surface sprays.[4] These alloys are used in submerged hardware in general galvanizing as well. Novel alloys designed for applications in submerged hardware frequently contain substantial amounts of Mo.[2,3] Hence, a detailed knowledge of the phase equilibrium in the Zn-Al-Mo system would be useful in understanding the corrosion mechanism of pot hardware and in the search for better materials for submerged hardware applications.

Molybdenum is also an important alloying element in high-strength steels for improved strength and increased resistance to hydrogen embrittlement. In galvanizing high-strength steels, Mo will dissolve from the steels and be enriched in the coating/substrate interface, thereby altering the thermodynamics and kinetics of the inhibition layer formation and affecting the coating quality. Molybdenum is also an important alloying element in 316L stainless steel, the material from which most pot rolls are made. The presence of Mo has a strong effect on the corrosion behavior of 316L stainless steel rolls in galvanizing. To fully understand the effects of Mo in steels on the galvanizing process and roll performance, knowledge of phase equilibria in the Zn-Fe-Al-Mo quaternary system is needed. Development of the Zn-Mo-Al phase diagram constitutes part of the authors' endeavor to develop the quaternary phase diagram.

2. Experimental Procedure

A total of 23 alloys containing Mo up to 40 at.% and Al up to 89 at.% was prepared using Zn, Al, and Mo metals in different forms. All metals had a purity of 99.99%. Thin discs of Zn cut from a rod using a diamond wheel were further cut into small pieces. Thin Al wire with a diameter of 0.8 mm was cut into fine pieces. Molybdenum powder was used in the experiment. Due to its extremely high melting point, the dissolution and diffusion of Mo in the alloy mixtures are expected to be slow during the melting and homogenizing treatments. Hence, a fine Mo powder is desirable for the experimental work. The Mo powder used in this study was only 74 μm in size (200 meshes). The total weight of each sample was 5 g. Samples were prepared by carefully weighing the Al, Zn, and Mo fines to an accuracy of 0.0001 g. The fines of the three metals were thoroughly mixed and wrapped in aluminum foil before being transferred to a quartz tube. The quartz tube was then evacuated and sealed under vacuum. Each alloy mixture was heated to 1200 °C and kept at this temperature for two days. The samples were water quenched at the end of this melting process. To minimize Zn loss during water quenching, a

Zhihong Wang, Jianhua Wang, and **Xuping Su,** Institute of Materials Research, School of Mechanical Engineering, Xiangtan University, Xiangtan 411105, Hunan, People's Republic of China; and **Nai-Yong Tang** and **Yi Hui Liu,** Teck Cominco Metals Ltd., Product Technology Centre, 2380 Speakman Dr., Mississauga, Ontario, L5K 1B4, Canada. Contact e-mail: sxping@xtu.edu.cn.

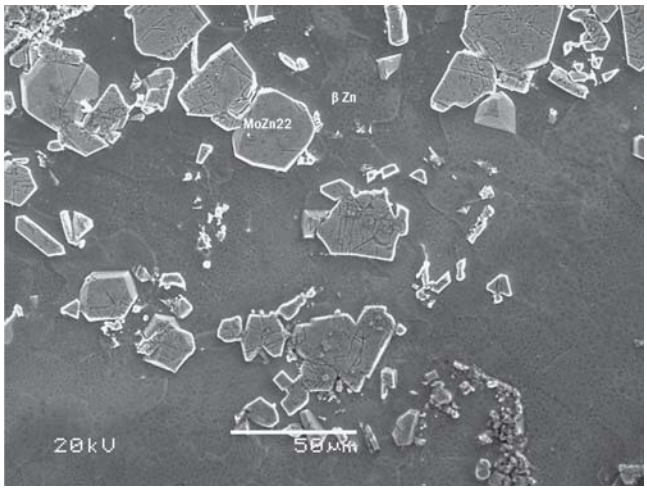

Fig. 1 Alloy 1 (96Zn-1Al-3Mo). The $MoZn_{22}$ compound coexists with the Zn solid-solution phase, the β phase.

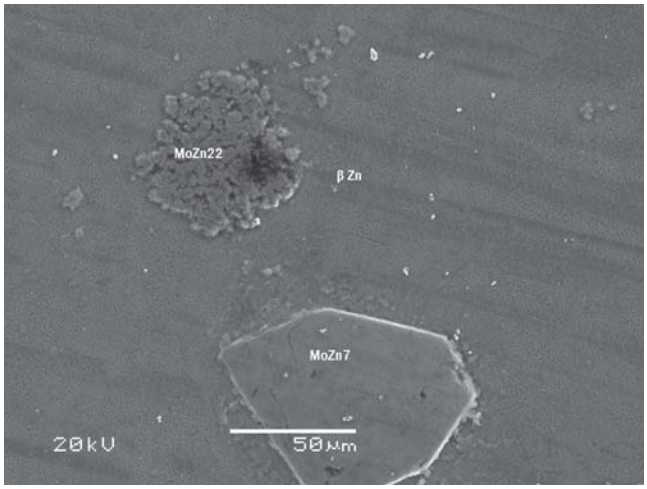

Fig. 2 Alloy 3 (94Zn-2Al-4Mo). $MoZn_{22}$ and $MoZn_7$ coexist with the β phase.

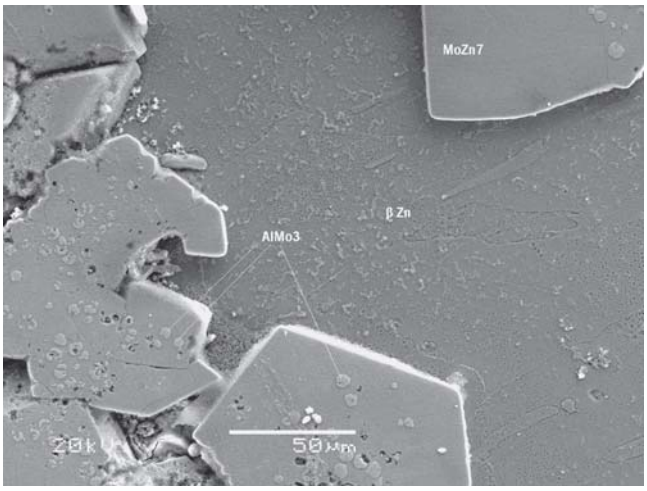

Fig. 3 The microstructure of alloy 5 (82Zn-13Al-5Mo) suggests an $AlMo_3$-$MoZn_7$-liquid three-phase equilibrium state at 450 °C.

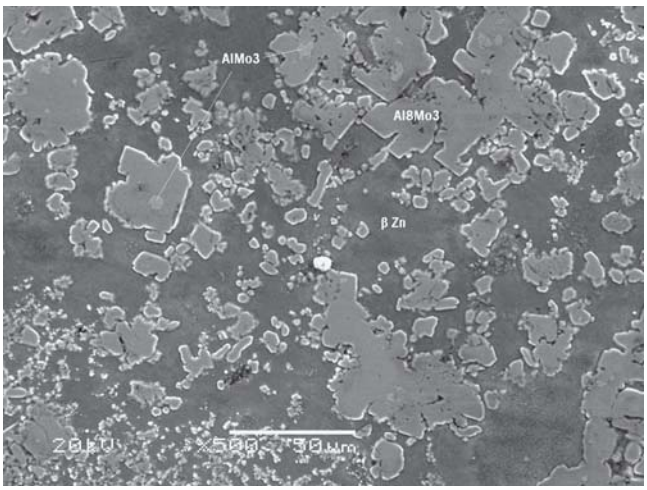

Fig. 4 The microstructure of alloy 8 (73Zn-27Al-4Mo) indicates that the $AlMo_3$ phase, the Al_8Mo_3 phase, and the liquid phase existed in a three-phase equilibrium state at 450 °C. Note: $AlMo_3$ particles exist within large Al_8Mo_3 particles.

special end-quenching technique invented by one of the authors and detailed elsewhere[5] was used. Most quartz capsules survived the quenching process; however, some capsules cracked. The samples in the cracked capsules were removed and put into new quartz capsules individually and sealed again under vacuum. All samples were then introduced into a furnace kept at 450 °C for 20 days. The samples were water quenched at the end of the treatment.

Sections of the specimens were prepared in the conventional way for metallographic examinations. A nital solution was used to reveal microstructural details. X-ray powder diffraction patterns were generated from samples using a Bruker D8 Advanced X-Ray Diffractometer (Bruker-AXS; Karlsruhe Germany, Madison WI), operating at 40 kV and 40 mA with Cu Kα radiation. Scanning electron microscopy-energy dispersive spectroscopy (SEM-EDS) analyses were performed in an SEM Model JSM-6360LV (JEOL, Tokyo, Japan) to study the morphology and the chemical compositions of various phases in the samples in the secondary electron (SE) mode. The operating voltage of the SEM was 20 kV.

3. Results and Discussion

The design compositions of the alloys are listed in Table 1. In general, the phases contained in an alloy reacted with the nital solution to different degrees and possessed different relief. Thus, phases can be easily differentiated based on the relief and the chemical compositions analyzed using the SEM-EDS technique. Nevertheless, an x-ray diffraction (XRD) study was carried out on every alloy investigated in this work, and the true identities of the phases were determined based on the XRD patterns.

The compositions of alloys 1 through 6 were located in the Zn-rich corner of the system. The microstructure of

Table 1 Compositions of all alloys and phases

Alloy	Design composition	Phase	Composition, wt.%		
			Zn	Al	Mo
1	96Zn-1Al-3Mo	$MoZn_{22}$	95.0	1.0	4.0
		βZn	99.0	1.0	…
2	93Zn-1Al-6Mo	$MoZn_7$	87.0	1.0	12.0
		$MoZn_{22}$	95.0	1.0	4.0
3	94Zn-2Al-4Mo	$MoZn_7$	86.0 ± 0.5	2.0 ± 0.5	12.0
		$MoZn_{22}$	95.0	12.0	4.0
		βZn	96.0 ± 0.5	4.0 ± 0.5	…
4	92Zn-6.5Al-1.5Mo	$MoZn_7$	82.0	6.0 ± 0.5	12.0 ± 0.5
		βZn	93.0 ± 0.5	7.0 ± 0.5	…
5	82Zn-13Al-5Mo	$AlMo_3$	13.0 ± 0.3	15.0 ± 0.2	72.0 ± 1
		$MoZn_7$	80.0	7.0	13.0
		βZn	85.0	15.0	…
6	80Zn-18.5Al-1.5Mo	$AlMo_3$	12.0	16.0	72.0
		βZn	81.0 ± 0.3	19.0 ± 0.3	…
7	79Zn-6Al-15Mo	$AlMo_3$	13.0	14.0	73.0
		$MoZn_7$	81.0	6.0	13.0
8	73Zn-23Al-4Mo	$AlMo_3$	12.5 ± 0.5	17.0	70.5 ± 0.5
		Al_8Mo_3	13.5 ± 0.5	60.0 ± 0.5	26.5
		βZn	78.0 ± 0.3	22.0 ± 0.3	…
9	71Zn-27Al-2Mo	Al_8Mo_3	13.0	60.0 ± 0.5	27.0 ± 0.5
		βZn	75.0	25.0	…
10	52Zn-45Al-3Mo	Al_8Mo_3	13.0	61.0	26.0
		βZn	72.0	28.0	…
		αAl	42.0	58.0	…
11	35Zn-62Al-3Mo	Al_8Mo_3	11.0 ± 0.3	64.0	26.0 ± 0.3
		αAl	38.0	62.0	…
12	27Zn-71Al-2Mo	Al_4Mo	8.0	72.0	20.0
		αAl	29.0	71.0	…
13	25.5Zn-74.5Al-6Mo	Al_8Mo_3	10.0	65.0	25.0
		Al_4Mo	8.0	72.0	20.0
		αAl	31.0	69.0	…
14	22.5Zn-72.5Al-5Mo	Al_4Mo	8.0	72.0	20.0
		Al_5Mo	5.0 ± 0.5	78.0 ± 0.5	17.0
		αAl	28.0	72.0	…
15	20Zn-76Al-4Mo	Al_5Mo	5.0	78.0	17.0
		αAl	24.0 ± 0.3	76.0 ± 0.2	…
16	15Zn-81Al-4Mo	Al_5Mo	5.0	78.0	17.0
		$Al_{12}Mo$	4.0	88.0	8.0
		αAl	20.0	80.0	…
17	9Zn-88Al-3Mo	$Al_{12}Mo$	3.5 ± 0.5	88.5 ± 0.5	8.0
		αAl	12.0 ± 0.5	88.0 ± 0.5	…
18	8Zn-60Al-32Mo	$AlMo_3$	2.0	25.0 ± 0.3	73.0 ± 0.3
		Al_8Mo_3	9.0 ± 0.2	62.0 ± 0.5	29.0 ± 0.3
19	6Zn-71Al-23Mo	Al_8Mo_3	6.0 ± 0.5	69.0 ± 0.5	25.0
		Al_4Mo	7.0 ± 0.3	73.0 ± 0.2	20.0
20	5Zn-77Al-18Mo	Al_4Mo	4.0 ± 0.2	76.0 ± 0.2	20.0
		Al_5Mo	5.0	78.0	17.0
21	2Zn-89Al-9Mo	Al_5Mo	4.0 ± 0.5	79.0 ± 0.5	17.0
		$Al_{12}Mo$	2.0 ± 0.3	90.0 ± 0.3	8.0
22	70Zn-4Al-27Mo	$MoZn_7$	83.0	4.0 ± 0.3	13.0 ± 0.5
		$AlMo_3$	13.0	14.0 ± 0.5	73.0 ± 0.5
		Mo	…	…	100.0
23	25Zn-40Al-35Mo	$AlMo_3$	10.0	18.0	72.0
		Al_8Mo_3	12.0	60.0	28.0
		βZn	76.0	24.0	…

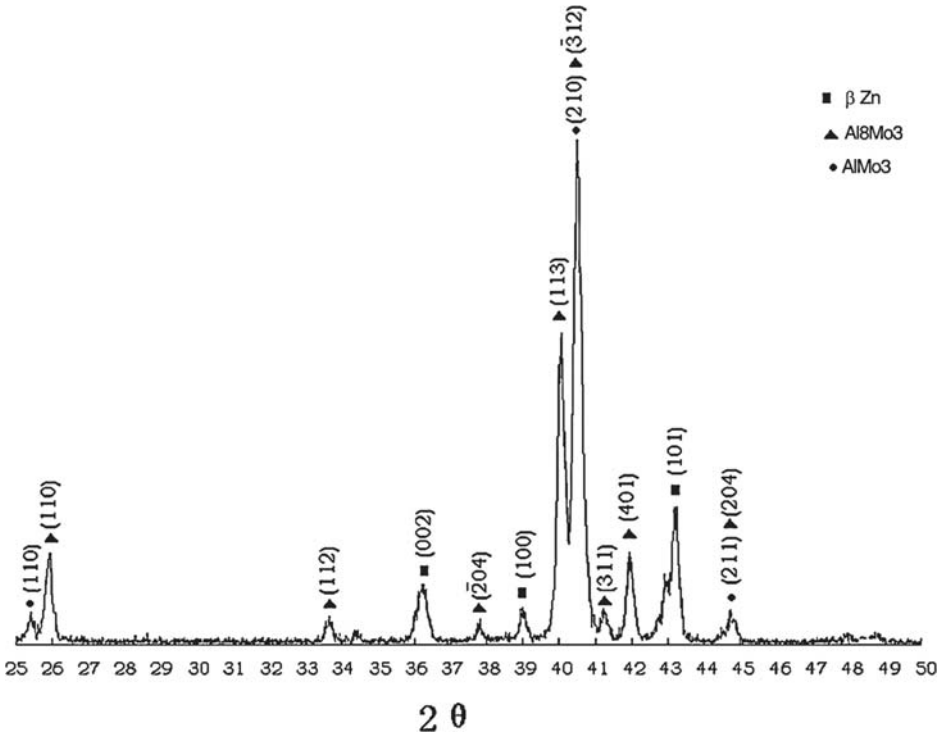

Fig 5 An x-ray powder diffraction pattern obtained from alloy 23 (25Zn-40Al-35Mo). Three phases, $AlMo_3$, Al_8Mo_3, and βZn, coexist in the alloy.

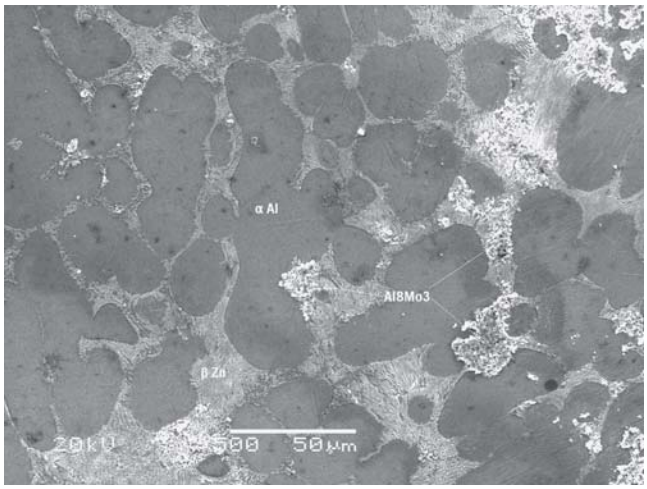

Fig. 6 Alloy 10 (52Zn-45Al-3Mo) consists of the Al_8Mo_3 phase, the βZn phase, and the αAl phase.

alloy 1 (96Zn-1Al-3Mo) consisted of a blocky phase embedded in the Zn-rich solid-solution phase, the β phase in Fig. 1; the β phase was in the liquid state at 450 °C. SEM-EDS analyses revealed that the blocky phase contained 95% Zn, 4% Mo, and 1% Al on average (all compositions are reported in atomic percentage in this study), suggesting that it is a ternary extension of the $MoZn_{22}$ phase. A study of the x-ray powder diffraction generated on the alloy confirmed that the phase is indeed the $MoZn_{22}$ phase. Molybdenum was not detected in the β phase. This indicates that the solubility of Mo in the liquid phase was negligible. The microstructure of alloy 2 (93Zn-1Al-6Mo) consisted of two compounds, the $MoZn_{22}$ phase and the $MoZn_7$ phase. Alloy 3 (94Zn-2Al-4Mo) consisted of three phases: the $MoZn_{22}$ phase, the $MoZn_7$ phase, and the β phase, as shown in Fig. 2. EDS analyses of this alloy indicated that the solubility of Al in $MoZn_7$ is slightly higher than that in $MoZn_{22}$. Alloy 4 (92Zn-6.5Al-1.5Mo) contained only 1.5% Mo, yet a large number of $MoZn_7$ particles were found in the alloy. This finding substantiates the authors' conclusion that Mo was almost insoluble in the liquid Zn. In alloy 5 (82Zn-13Al-5Mo), a new phase, the $AlMo_3$ phase, appeared. As shown in Fig. 3, $AlMo_3$ particles existed mostly within bulky $MoZn_7$ particles. The alloy consists of the $MoZn_7$ phase, the $AlMo_3$ phase, and the β phase, corresponding to a three-phase equilibrium state. Alloy 6 (80Zn-18.5Al-1.5Mo) consisted of the $AlMo_3$ phase and the β phase, and alloy 7 (79Zn-6Al-15Mo) consisted of the $AlMo_3$ phase and $MoZn_7$ phase. SEM-EDS analyses of the β phase in these alloys suggest that the Al content of the liquid phase at 450 °C increased with the increased Al content of the alloys, ranging from 1 at.% in alloy 1 (96-Zn-1Al-3Mo) to 19 at.% for alloy 6 (80Zn-18.5Al-1.5Mo). The Al content of the $MoZn_7$ compound also increased with the increased Al content of the alloys, ranging from 1% for alloy 2 (93Zn-1Al-6Mo) to 7% for alloy 5 (82Zn-13Al-5Mo). On the other hand, the Al solubility in the $MoZn_{22}$ compound was maximized at 1% in alloy 3 (94Zn-2Al-4Mo).

The microstructure of alloy 8 (73Zn-23Al-4Mo) is shown in Fig. 4. It consists of three phases: the Al_8Mo_3 phase existing as particles embedded in the β matrix and

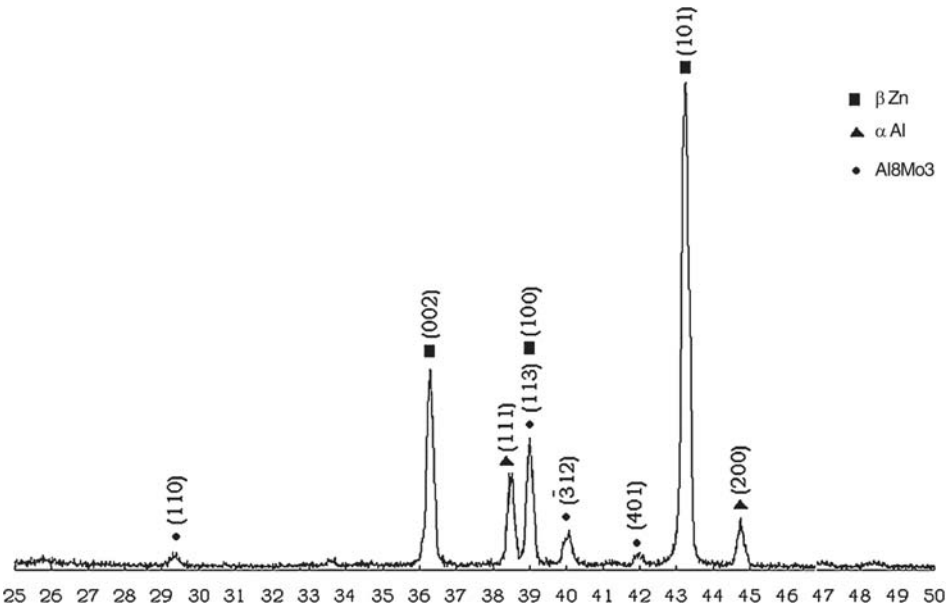

Fig. 7 The XRD pattern generated from alloy 10 (52Zn-45Al-3Mo) reveals that three phases, the Al_8Mo_3, the βZn, and the αAl, coexist.

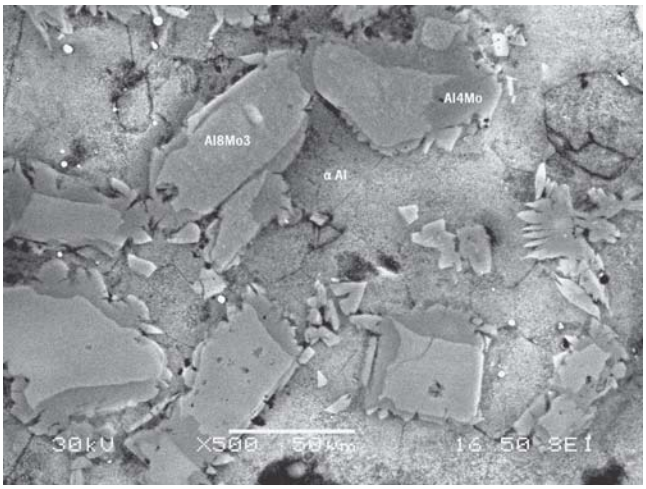

Fig. 8 Alloy 13 (25.5Zn-74.5Al-6Mo) consists of a mixture of αAl and Al_8Mo_3 surrounded frequently by the Al_4Mo compound.

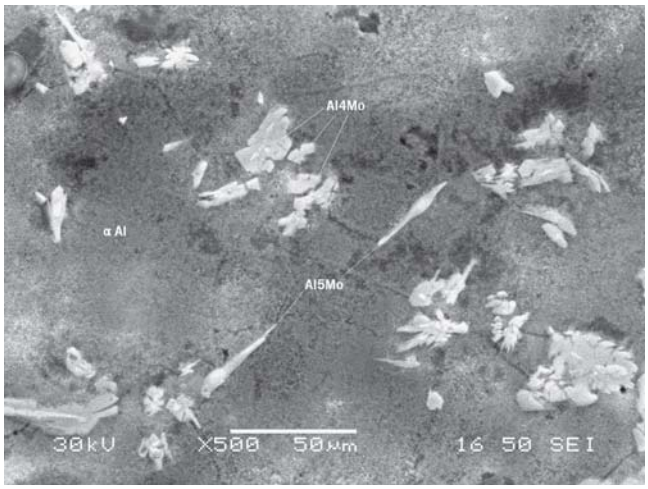

Fig. 9 Alloy 14 (22.5Zn-72.5Al-5Mo) consists of Al_4Mo, and Al_5Mo existed in the αAl matrix. The αAl was decomposed.

small spherical particles of the $AlMo_3$ phase existing mainly within large Al_8Mo_3 particles. Because this three-phase triangle covers a rather wide area, alloy 23 (25Zn-40Al-35Mo) was prepared to further confirm the existence of this three-phase equilibrium state. SEM-EDS and XRD analyses indicated that these two alloys consist of the same phases: Al_8Mo_3, $AlMo_3$, and β phases. An XRD pattern generated for alloy 23 is shown in Fig. 5. The characteristic peaks of the Al_8Mo_3 phase, the $AlMo_3$ phase, and the β phase have been identified. The Zn solubility limits in the $AlMo_3$ and Al_8Mo_3 compounds were 11.5% and 13.5%, respectively.

The Al_8Mo_3 compound coexisted with the β phase in alloy 9 (71Zn-27Al-2Mo). A new three-phase equilibrium state involving the Al_8Mo_3 phase, the β phase, and the Al-rich solid-solution phase α was observed in alloy 10 (52Zn-45Al-3Mo), as shown in Fig. 6. The corresponding x-ray powder diffraction pattern is shown in Fig. 7. The coexistence of the Al_8Mo_3 phase, the β phase, and the α phase is clearly demonstrated in these figures. The morphology of the β phase shown in Fig. 6 suggests that the liquid decomposed into a very fine eutectic microstructure instead of solidifying into the Zn-rich solid-solution phase during water quenching. As a result, the Al content in the β phase reported in Table 1 is the mean value of that of the eutectic. It appears that the liquid phase in alloys 4 to 6, 8, 9, and 23 has also partly decomposed during quenching, although the resultant eutectic microstructure is much finer. The Al_8Mo_3

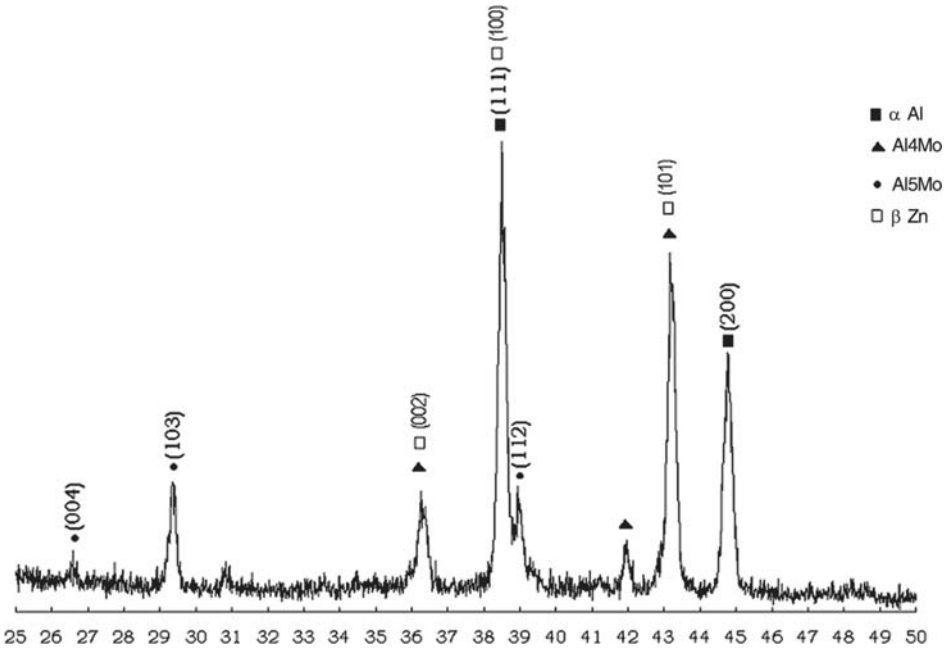

Fig. 10 An XRD pattern generated from alloy 14 (22.5Zn-72.5Al-5Mo)

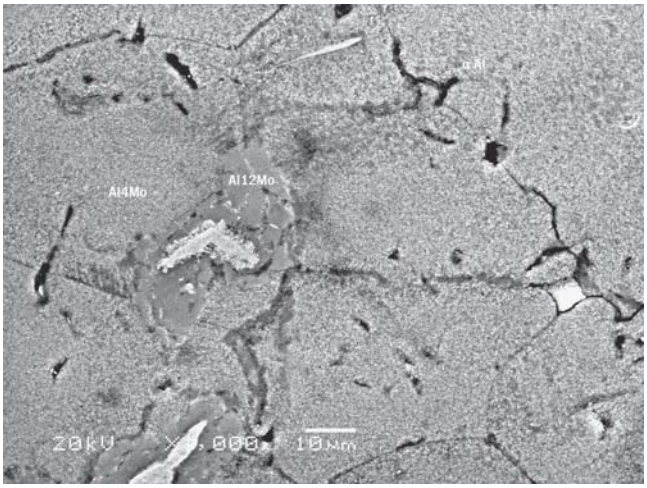

Fig. 11 Alloy 16 (15Zn-81Al-4Mo) consists of Al_5Mo, $Al_{12}Mo$, and αAl. $Al_{12}Mo$ particles are etched dark gray and Al_5Mo particles are etched lighter gray.

phase coexisted with the α phase in alloy 11 (35Zn-62Al-3Mo), while the Al_4Mo phase coexisted with the α phase in alloy 12 (27Zn-71Al-2Mo). With further increases in the Al content of the alloys, more Mo aluminides were encountered. Alloy 13 (25.5Zn-72.5Al-5Mo) consisted of three phases: the Al_8Mo_3 phase, the Al_4Mo phase, and the αAl phase, as shown in Fig. 8. The microstructure of alloy 14 (22.5Zn-72.5Al-5Mo) is shown in Fig. 9 with its corresponding x-ray powder diffraction pattern in Fig. 10. SEM-EDS analyses and XRD studies indicated that three phases, Al_4Mo, Al_5Mo, and αAl, existed in this alloy. Al_4Mo particles were blocky in shape, and Al_5Mo particles were irregular. The microstructure and the XRD pattern suggest that the α phase was partly decomposed because the αAl phase in Fig. 9 appeared mottled, and all three major peaks of Zn exist in the x-ray pattern, overlapping with the peaks contributed by the intermetallic compounds. Decomposition of the α phase that was initially supersaturated with Zn could be the result of a sluggish quenching process at the end of the homogenizing treatment. Another possibility is that the α phase supersaturated with Zn is not stable at room temperature. Zinc is a metal with a low melting point. Its diffusivity in the α phase at room temperature is significant, resulting in the decomposition of the supersaturated solid solution. Alloy 16 (15Zn-81Al-4Mo) was found to consist of three phases: Al_5Mo, $Al_{12}Mo$, and α, as shown in Fig. 11. $Al_{12}Mo$ particles are etched dark gray, and Al_5Mo particles are lighter gray. Again, the α phase in this sample is partly decomposed.

All phases found in the alloys are summarized in Table 1 together with their chemical compositions determined using the SEM-EDS technique. The compositions listed are the averages over at least six measurements.

Based on the findings described in this article, the 450 °C isothermal section of the Zn-Al-Mo system is proposed in Fig. 12. The binary sides of the isothermal section were drawn based on the information available in the open literature. The Al-Zn system is well studied. It is a eutectic system involving a monotectoid reaction and a miscibility gap in the solid state.[6] Since 1897, the liquidus curve of the α phase has been repeatedly determined by several researchers,[7-12] although there is still some uncertainty on the position of the αAl phase boundary. The phase boundaries in the prevailing Zn-Al phase diagram are drawn based on microscopic studies.[9,10,13-15] To determine the solidus curve of the α phase, Ellwood[16] carried out high-temperature x-ray analysis. The solubility limits in the as-

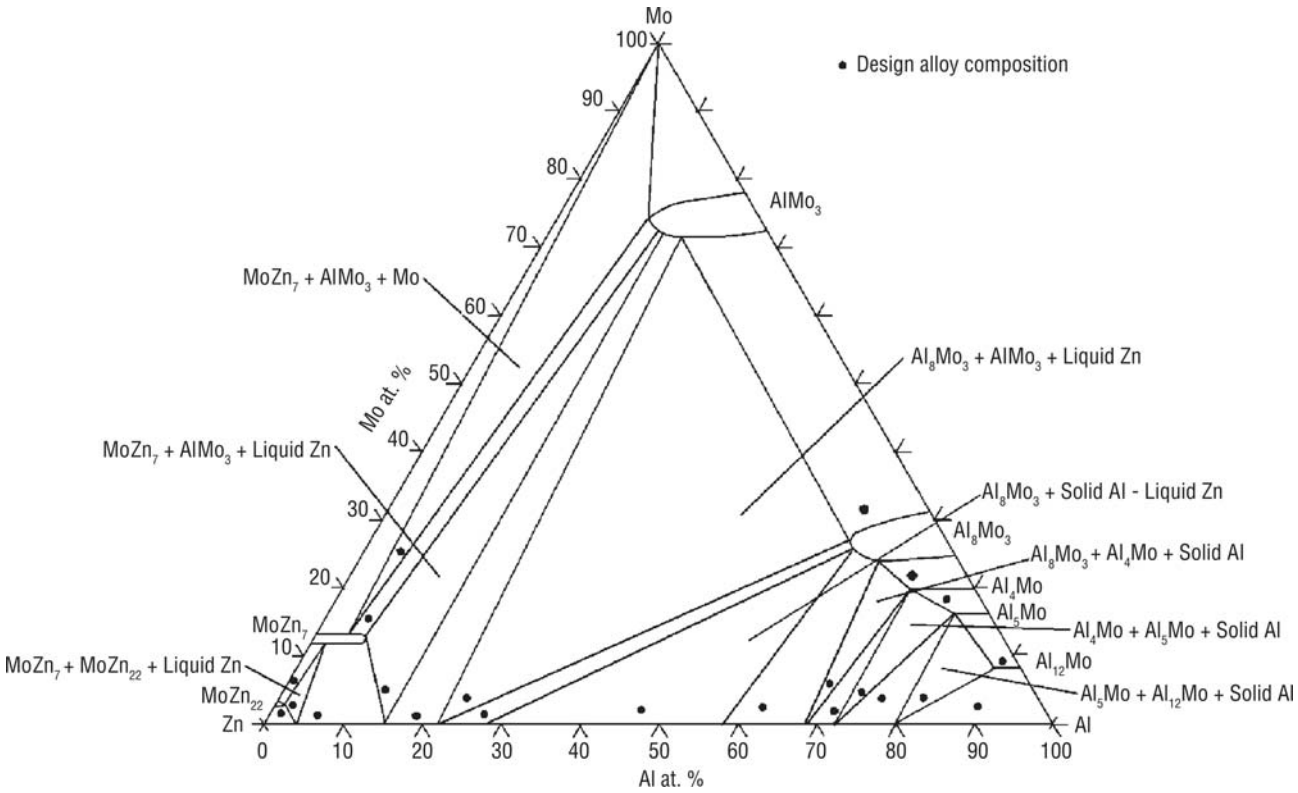

Fig. 12 The 450 °C isothermal section of the Zn-Al-Mo ternary phase diagram. The black dots in the diagram mark the alloy compositions studied in this work.

sessed phase diagram are based on resistivity measurement data of Fink[17] and others.[18,19] The low-temperature solubilities are linear extrapolations of experimental data obtained by Auer and Mann,[20] Loehberg,[21] and Hofmann and Fahrenhorst.[22]

The Al-Mo phase diagram[23] is constructed based on the data of Walford,[24] Petzow and Rexer,[25] and Rexer.[26] According to these studies, there are only five Al-Mo binary intermetallic compounds in the system, that is, $Al_{12}Mo$, Al_5Mo, Al_4Mo, Al_8Mo_3, and $AlMo_3$. However, other researchers[27] suggest the existence of five additional aluminides, namely Al_6Mo, $Al_{22}Mo_5$, $Al_{17}Mo_4$, $Al_{63}Mo_{37}$, and AlMo. The current study found the existence of liquid-Al_8Mo_3-$AlMo_3$ three-phase equilibrium in alloys 8 and 23 and the coexistence of the Al_8Mo_3-$AlMo_3$ two-phase equilibrium in alloy 18. The tie triangle of the liquid-Al_8Mo_3-$AlMo_3$ three phases in Fig. 12 is outlined based on the average phase compositions of alloy 23 instead of alloy 8. This is because the volume fractions of the Al_8Mo_3 and $AlMo_3$ phases are larger in alloy 23 than in alloy 8, and the phase composition measurements are deemed more accurate. The current study failed to detect the existence of AlMo and $Al_{63}Mo_{37}$ phases, suggesting that these two compounds are probably stable only at much higher temperatures. The ternary extensions of the five intermediate phases—that is, $Al_{12}Mo$, Al_5Mo, Al_4Mo, Al_8Mo_3, and $AlMo_3$—identified by Saunders,[23] were all positively identified in the current study. It should be mentioned here that analyses of x-ray patterns obtained in this study suggest that the $Al_{22}Mo_5$ phase may exist. However, the XRD patterns were complex; the characteristic peaks of the compounds were weak. In addition, the compounds of Al_5Mo, $Al_{22}Mo_5$, and Al_4Mo all contain Zn in solid solution, and analyses using the SEM-EDS technique contain some uncertainty. These factors made a positive identification of the compound difficult. The interest of the current study lies mainly in the Zn-rich corner of the system; such an uncertainty in the isothermal section does not affect the intended practical application of the phase diagram.

The Mo-Zn phase diagram was calculated based on a thermodynamic model derived primarily from the data of Martin et al.[28] There are two intermediate phases, namely $MoZn_{22}$ and $MoZn_7$, in this system. Ternary extensions of these two phases were found in the Zn-rich corner of the Zn-Al-Mo system in the current study.

The liquid phase boundary and the α phase boundary almost overlap with the Zn-Al binary side in Fig. 12 because the Mo solubility in these two phases is negligible. The liquid α two-phase region is drawn based on the existing Zn-Al phase diagram and experimental data obtained in this study. The vertices of all three-phase triangles were drawn based on the experimental results obtained in this study. In the Zn-rich corner, it can be seen that the liquid phase is in equilibrium with ternary extensions of the two binary Zn-Mo intermetallic compounds, namely $MoZn_{22}$ and $MoZn_7$, for Al contents up to 17% and in equilibrium with extensions of the $AlMo_3$ and Al_8Mo_3 phases with a further increase in the Al content of the alloy.

4. Conclusions

Based on the microstructures of the alloys and the phase compositions determined using the SEM-EDS technique, phase equilibrium states available in the Zn-Al-Mo ternary system at 450 °C were determined. These conclusions can be drawn:

- In the Zn-rich corner of the system, the liquid phase is in equilibrium with the extension of the binary $MoZn_{22}$ phase for Al content up to 5% and with that of the $MoZn_7$ phase for Al content up to 17%. The Mo solubility in the liquid phase was not detectable using the SEM-EDS technique.
- When the Al content of the alloys exceeds 17%, but is less than 28%, the liquid phase is in equilibrium with the ternary extensions of the binary $AlMo_3$ and Al_8Mo_3 phases. The Zn solubility in the $AlMo_3$ and Al_8Mo_3 compounds was 13.0% and 13.5%, respectively.
- Among the two Mo-Zn intermetallic compounds, only the $MoZn_7$ phase can coexist with the $AlMo_3$ phase because the Al solubility in the $MoZn_7$ compound is much higher than that in the $MoZn_{22}$ compound, being 7% and 1%, respectively.
- The Al-rich solid-solution phase, the α phase, is in equilibrium with Al_8Mo_3, Al_4Mo, Al_5Mo, and $Al_{12}Mo$. The solubility of Mo in the α phase is negligible.

Acknowledgments

The authors would like to acknowledge the financial support provided by the Natural Science Foundation of China (No. 50471064), NCET (04-0778), and Teck Cominco Metals Ltd. of Canada.

References

1. A.R. Marder, A Review of the Metallurgy of Zinc Coated Steel, *Prog. Mater. Sci.,* 2000, **45,** p 191-271
2. K. Zhang and N.-Y. Tang, Reactions of Co-Based and Fe-Based Superalloys with a Molten Zn-Alloy, *Mater. Sci. Technol.,* 2004, **20**(6), p 739-746
3. K. Zhang and N.-Y. Tang, On the Wear of a Cobalt-Based Superalloy in Zinc Baths, *Metall. Mater. Trans A,* 2003, **34A,** p 2387-2396
4. H.H. Fukubayashi, "Present Furnace and Pot Roll Coatings and Future Development," Proceedings, Galvanizers Association Meeting (Portland, OR), Oct 2001
5. X. Su, N.Y. Tang, and J.M. Toguri, 450 °C Isothermal Section of the Fe-Zn-Si Ternary Phase Diagram, *Can. Metall. Q.,* 2001, **40**(33), p 377-384
6. J.L. Murray, The Al-Zn System, *Bull. Alloy Phase Diagrams,* 1983, June, 4(1), p 17-18
7. C.T. Heycock and F.H. Neville, *J. Chem. Soc.,* 1897, **71,** p 383-385
8. T. Isihara, On the Equilibrium Diagram of the Aluminum-Zinc System, *Sci. Rep. Tohoku Univ.,* 1925, **13,** p 427-442
9. M.L.V. Gayler, M. Haughton, and E.G. Sutherland, Constitution of Aluminum-Zinc Alloys of High Purity; Nature of Thermal Change at 443 °C, *J. Inst. Met.,* 1938, **63**(2), p 80
10. E. Butchers and W. Hume-Rothery, On Constitution of Aluminum-Magnesium-Manganese-Zinc Alloys: Solidus, *J. Inst. Met.,* 1945, **71,** p 291-311
11. E. Pelzel, Liquidus and Solidus Curves in Zinc Aluminum System Between 30 and 70% Aluminum, *Z. Metallkd.,* 1949, **40**(4), p 134-136
12. I.S. Solet and W.W. St. Clair, "Bureau of Mines Report of Investigations," 1949, p 4553
13. D. Hanson and M.L. Gayler, A Further Study of the Alloys of Aluminum and Zinc, *J. Inst. Met.,* 1922, **27,** p 28
14. T. Morinaga, *Nippon Kinzoku Gakkaishi,* 1939, **3,** p 216-220
15. E. Gebhardt, Equilibrium Studies of Systems Zinc Aluminum and Zinc Aluminum Copper, *Z. Metallkd.,* 1949, **40**(4), p 136-140, in German
16. E.C. Ellwood, Solid Solutions of Zinc in Aluminum, *J. Inst. Met.,* 1951, **80**(5), p 217-224
17. W.L. Fink, Equilibrium Relations in Aluminum-Zinc Alloys of High Purity-II, *Trans. AIME,* 1936, **12,** p 244-260
18. G. Borelius and L.E. Larsson, *Ark. Mat. Astr. Fys.,* 1948, **35A**(13), p 1-5
19. L.E. Larsson, Pre-Precipitation and Precipitation Phenomena in Al-Zn System, *Acta Metall.,* 1967, **15**(1), p 35-44
20. H. Auer and K.E.M. Mann, Magnetic Investigation of Zinc Aluminum System, *Z. Metallkd.,* 1936, **28**(10), p 323-326, in German
21. K. Loehberg, X-ray Determination of Solubility of Aluminum and Copper in Zinc, *Z. Metallkd.,* 1940, **32**(4), p 86-90, in German
22. W. Hofmann and G. Fahrenhorst, *Z. Metallkd.,* 1950, **42,** p 460-463, in German
23. N. Saunders, Al-Mo (Aluminum-Molybdenum), *Binary Alloy Phase Diagrams,* 2nd ed., T.B. Massalski, Ed., ASM International, 1990, p 174-175
24. L.K. Walford, The Structure of the Intermetallic Phase $MoAl_{12}$, $ReAl_{12}$, and $TcAl_{12}$, *Philos. Mag.,* 1964, **9,** p 57-62
25. G. Petzow and J. Rexer, Melting Equilibrium System U-UA_{12}-Al8Mo_3-Mo, *Z. Metallkd.,* 1969, **60**(5), p 449-453
26. J. Rexer, Phase Equilibria in the Al-Mo System Above 1400 °C, *Z. Metallkd.,* 1971, **62**(11), p 844-848
27. L. Brewer and R.H. Lamoreaux, II. Phase Diagrams, Atomic Energy Rev., Spec. Issue No. 7, *Molybdenum: Physico-Chemical Properties of Its Compounds and Alloys,* International Atomic Energy Agency, Vienna, Austria, 1980, p 204-208
28. A.E. Martin, J.B. Knighton, and H.M. Feder, *J. Chem. Eng. Data,* 1961, p 598